Properties and application of a multichannel integrated circuit for low-artifact, patterned electrical stimulation of neural tissue

2012 J. Neural Eng. 9 066005

(http://iopscience.iop.org/1741-2552/9/6/066005)

J. Neural Eng. **9** (2012) 066005 (17pp) doi:10.1088/1741-2560/9/6/066005

Properties and application of a multichannel integrated circuit for low-artifact, patterned electrical stimulation of neural tissue

Paweł Hottowy[1,2], Andrzej Skoczeń[1], Deborah E Gunning[3], Sergei Kachiguine[2], Keith Mathieson[3], Alexander Sher[2], Piotr Wiącek[1], Alan M Litke[2,4] and Władysław Dąbrowski[1,4]

[1] Faculty of Physics and Applied Computer Science, AGH University of Science and Technology, al. Mickiewicza 30, 30-059 Krakow, Poland
[2] Santa Cruz Institute for Particle Physics, University of California, Santa Cruz, 1156 High Street, Santa Cruz, CA 95064, USA
[3] School of Physics and Astronomy (SUPA), University of Glasgow, Glasgow G12 8QQ, UK

E-mail: hottowy@agh.edu.pl

Received 10 July 2012
Accepted for publication 11 October 2012
Published 16 November 2012
Online at stacks.iop.org/JNE/9/066005

Abstract
Objective. Modern multielectrode array (MEA) systems can record the neuronal activity from thousands of electrodes, but their ability to provide spatio-temporal patterns of electrical stimulation is very limited. Furthermore, the stimulus-related artifacts significantly limit the ability to record the neuronal responses to the stimulation. To address these issues, we designed a multichannel integrated circuit for a patterned MEA-based electrical stimulation and evaluated its performance in experiments with isolated mouse and rat retina. *Approach*. The Stimchip includes 64 independent stimulation channels. Each channel comprises an internal digital-to-analogue converter that can be configured as a current or voltage source. The shape of the stimulation waveform is defined independently for each channel by the real-time data stream. In addition, each channel is equipped with circuitry for reduction of the stimulus artifact. *Main results*. Using a high-density MEA stimulation/recording system, we effectively stimulated individual retinal ganglion cells (RGCs) and recorded the neuronal responses with minimal distortion, even on the stimulating electrodes. We independently stimulated a population of RGCs in rat retina, and using a complex spatio-temporal pattern of electrical stimulation pulses, we replicated visually evoked spiking activity of a subset of these cells with high fidelity. *Significance*. Compared with current state-of-the-art MEA systems, the Stimchip is able to stimulate neuronal cells with much more complex sequences of electrical pulses and with significantly reduced artifacts. This opens up new possibilities for studies of neuronal responses to electrical stimulation, both in the context of neuroscience research and in the development of neuroprosthetic devices.

(Some figures may appear in colour only in the online journal)

[4] A M L and W D contributed equally.

1. Introduction

Multielectrode array (MEA) systems for electrical interfacing with networks of living neurons have proven to be very attractive tools for neuroscience research and biosensing applications. These systems can record the activity of a large number of neurons simultaneously, both *in vitro* and *in vivo*, as well as stimulate this activity by injecting electrical currents into the extracellular medium. The current state-of-the-art systems use large-scale MEAs with electrode diameters and interelectrode spacings approaching the size and spacing of neurons (Csicsvari *et al* 2003, Eversmann *et al* 2003, Litke *et al* 2004, Berdondini *et al* 2005, Blanche *et al* 2005, Frey *et al* 2010). Since the signal amplitudes sensed by extracellular electrodes are in general of the order of a few hundred μV or lower, these systems require dedicated low-noise, high-gain readout circuitry. The readout electronics is usually designed in the form of a dedicated multichannel integrated circuit that is bonded to the array (Dąbrowski *et al* 2005, Charvet *et al* 2010; for a review, see Jochum *et al* 2009) or integrated with the MEA on a single chip (Eversmann *et al* 2003, Berdondini *et al* 2005, Frey *et al* 2010). Such systems are able to record the activities of a large number of closely spaced neurons in parallel and they open up new possibilities for the investigation of information processing in local neural networks (Petrusca *et al* 2007, Fujisawa *et al* 2008, Pillow *et al* 2008, Tang *et al* 2008, Field *et al* 2010).

However, in contrast to the capability of modern MEA-based systems to record complex spatio-temporal neural network activity patterns, the functionality of these systems with respect to the electrical stimulation of complex neuronal activity is very limited. The stimulation is usually restricted to a single electrode, or several electrodes following the same stimulation protocol (Dąbrowski *et al* 2004). More sophisticated approaches include the definition of several independent stimulation signals that can be repeated by groups of electrodes (Charvet *et al* 2010, Frey *et al* 2010) or the fast switching of single-channel stimulation circuitry between electrodes (Wagenaar *et al* 2004). Although these systems can generate patterns of stimulation signals that are distributed in space and time, none of them exploits the potential of modern MEAs to elicit complex, arbitrarily defined activity patterns in a large number of neurons.

An additional problem common to all systems aiming at simultaneous electrical stimulation and recording is the stimulation artifact. The electrical signals applied to activate neurons are sensed by all electrodes of the array as stimulus-related artifacts, with amplitudes several orders of magnitude larger than the amplitudes of the recorded action potentials. This can result in the saturation of the recording amplifier and makes the detection of the neuron response very difficult. Although the artifact can be vastly reduced by the optimization of the stimulation circuitry and experimental protocol (Jimbo *et al* 2003, Brown *et al* 2008, Frey *et al* 2010), as well as by additional signal post-processing during data analysis (Wichmann 2000, Wagenaar and Potter 2002, Gnadt *et al* 2003, Sekirnjak *et al* 2006), current MEA systems are unable to record neuronal responses on the stimulating electrode for at least two milliseconds following the stimulus, and for at least half a millisecond on the nearby non-stimulating electrodes. In comparison, the delay of the elicited action potential in response to the stimulation pulse can be as short as 100 μs (Sekirnjak *et al* 2008) and the duration of the recorded pulse is of the order of a millisecond. Therefore, the detection and proper identification of fast neuronal responses with such systems are extremely difficult.

In this paper, we describe the design and application of the Stimchip—an application-specific integrated circuit (ASIC) designed for a low-artifact stimulation of a population of neurons with complex patterns of stimulation signals, defined arbitrarily in space and time. We present an application of the chip to the stimulation of rodent retinal ganglion cells (RGCs) using a high-density MEA and an optimized stimulation pulse waveform. Finally, we demonstrate that the Stimchip allows for the elicitation of arbitrarily defined sequences of spikes in a population of neurons and makes possible the recording of the elicited short-latency spikes with minimal artifact-related distortions, even on the electrodes used for the stimulation.

2. Materials and methods

2.1. Design of the stimulation circuitry

A functional schematic diagram of a single Stimchip channel is shown in figure 1(A). The channel comprises a programmable bipolar current source to generate current stimulation signals of either polarity, a current-to-voltage converter that allows the generation of the stimulation signals in the voltage mode and switching circuitry for artifact suppression. The basic specification parameters are summarized in figure 1(C).

The current source is controlled by an internal 7 bit digital-to-analogue converter (DAC). The DAC design is based on binary weighted current sources and provides unipolar current from 0 to 250 μA. The DAC output current waveform is defined by a stream of real-time data received continuously from the off-chip controller. The data stream specifies, independently for each ASIC channel, the stimulation signal level for each 50 μs sampling period, with 7 bits to specify the amplitude and 1 bit to specify the polarity. It is thus possible to generate complex patterns of stimulation pulses, with both the stimulation signal waveforms and the spatio-temporal distribution of the pulses defined arbitrarily by the user. The DAC output signal is scaled in one of eight selectable output current buffers to match the required current range (see figure 1(C)). The bipolar current pulse from the selected buffer is finally sent to the electrode, either directly—if the current stimulation mode is selected—or via the current-to-voltage converter. In the latter case, the stimulation signal amplitude is additionally corrected for the electrode offset held on the 10 pF hold capacitor (Jimbo *et al* 2003). The amplitude range and the mode of stimulation (current versus voltage) are defined prior to the experiment, independently for each channel, by sending appropriate commands to the chip. For details of the design of the DAC, the output current buffers and the current-to-voltage converter, see Hottowy *et al* (2008b).

The artifact suppression circuit follows the idea proposed by Jimbo *et al* (2003) and consists of a hold capacitor, a

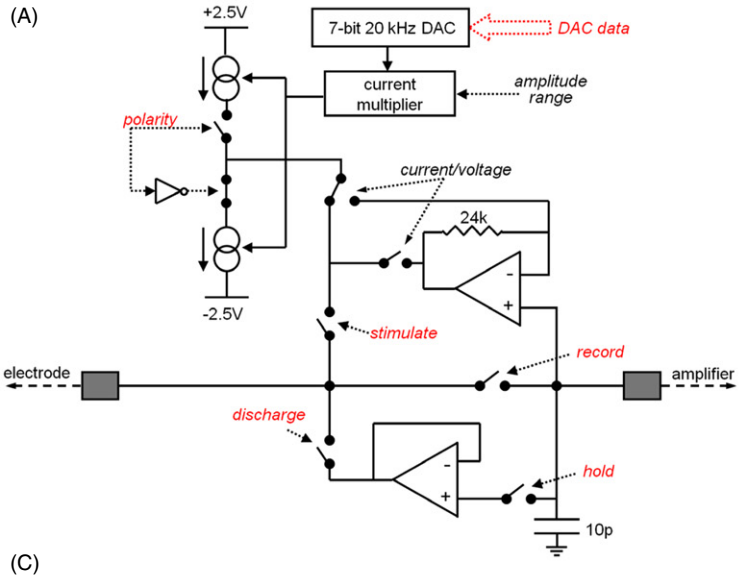

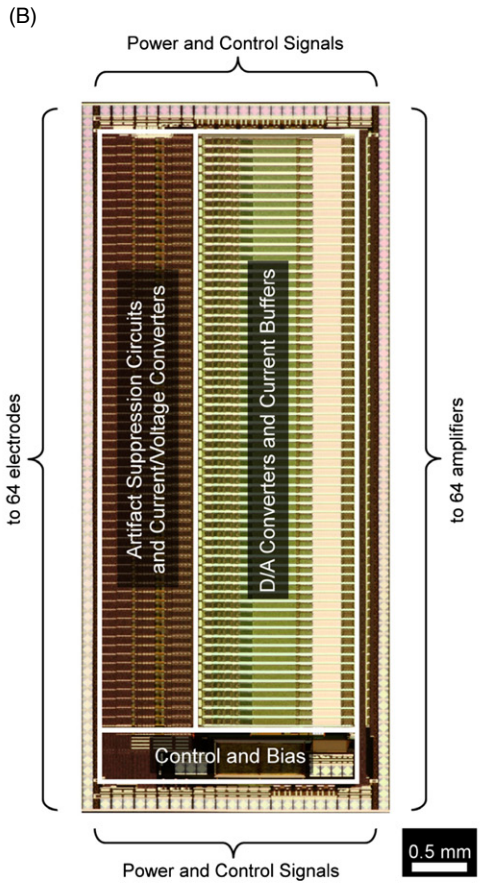

(C)

Parameter	Value
Supply voltage for analogue circuits	+/-2.5 V
Supply voltage for chip logic	+0.8/-2.5 V
Number of channels	64
Pitch of input/output pads	100 μm
Stimulation current ranges	+/- 60 nA, 250 nA, 1 μA, 4 μA, 16 μA, 64 μA, 260 μA, 1 mA
Stimulation voltage ranges	+/- 1.5 mV, 6 mV, 25 mV, 100 mV, 380 mV, 1.5 V
Resolution of the stimulation current	8 bits in each current range (including polarity bit)
Resolution of the stimulation voltage	8 bits in each voltage range (including polarity bit)
Time resolution of stimulation waveform	50 μs
Chip address	5 bits

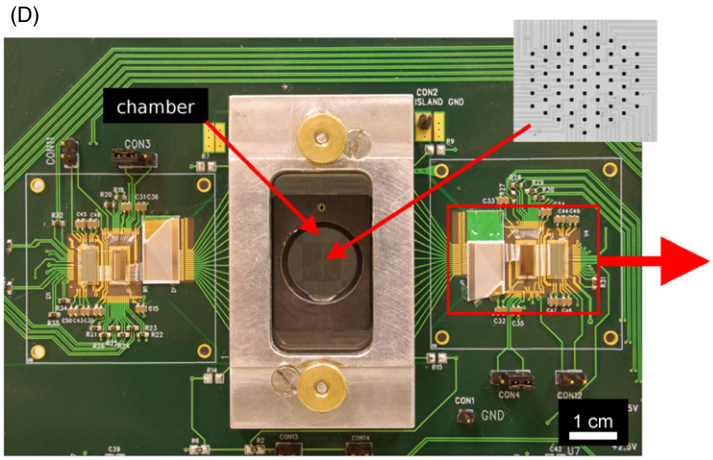

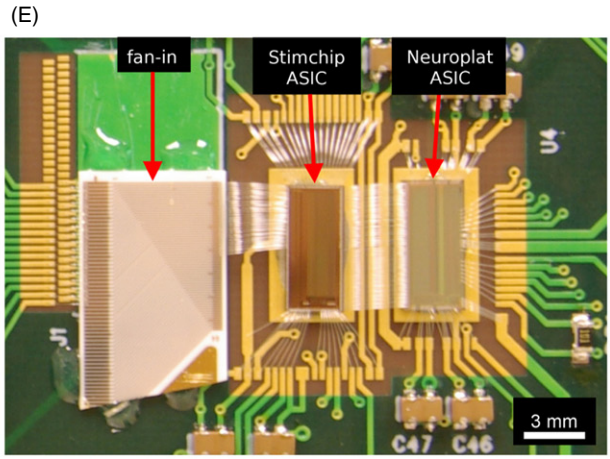

Figure 1. Stimchip design. (A) Schematic functional diagram of a stimulation channel. The control signals are labeled in italic font. The signals controlled in real time are labeled in red. (B) Microphotograph of the chip. The die area is 6.4 × 2.8 mm^2. (C) Basic parameters of the chip. (D) The central section of the PCB that includes the recording chamber, the 61-electrode MEA and two Stimchip/Neuroplat pairs with fan-ins. The inset shows the photograph of the MEA. The interelectrode distance is 60 μm. (E) Magnified view of a fan-in (pitch adapter) and the Stimchip and Neuroplat chips assembled on the PCB. The wire-bond connections between the Stimchip, the fan-in and the Neuroplat chip are visible.

tracking amplifier of gain equal to 1 and three switches controlled by three logic signals: *record, discharge* and *hold.* The *record* switch is used to disconnect the recording amplifier from the electrode while the stimulation pulse is generated. When this switch is open, the electrode pre-stimulation potential is stored on the hold capacitor and connected to the input of the recording amplifier.

For cancellation of the charge left at the electrode–electrolyte interface by the stimulation pulse, the electrode is connected to the tracking amplifier output (*discharge* = ON) that reproduces the electrode pre-stimulation potential. During the discharging phase, the amplifier is disconnected from the electrode (*record* = OFF). The discharging period can be adjusted in 50 μs steps to find the optimal compromise

between the minimization of the remaining residual artifact and the reduction of the delay between the stimulation pulse and the moment when the amplifier is reconnected to the electrode. The transistors used in the *discharge* switch must be relatively large to ensure low impedance of the closed switch and therefore a fast discharge time. In order to avoid parasitic charge injection from the *discharge* switch to the recording amplifier input through the feedback loop and input capacitance of the voltage follower, the *hold* switch can be used to separate the input of the recording amplifier from the tracking amplifier during the discharging phase; in such a configuration, the input voltage for the recording amplifier is stored only at the input capacitance of the tracking amplifier. Details of the artifact cancellation circuitry design are described by Hottowy *et al* (2008b).

2.2. Stimulation protocol

When a given stimulation channel is not active, the electrode is connected to the recording amplifier (signal *record* = *ON*) and both the stimulation signal source and the artifact suppression circuitry are disabled (*stimulate* = *OFF*, *discharge* = *OFF*, *hold* = *ON*). In this configuration, the signal sensed by the electrode is continuously recorded by the amplifier.

If the stimulation channel is enabled, the *record, stimulate, hold* and *discharge* switches, as well as the DAC and polarity settings, are controlled in real-time in 50 μs time steps by a stream of external data. For measurements employing the same electrode for the stimulation and recording, the standard protocol is as follows.

(1) Before the stimulation, the amplifier is connected to the electrode and the neuronal signals are recorded continuously.
(2) In the first stage of stimulation, the amplifier gets disconnected from the electrode (by setting *record* = *OFF*) and the amplifier input potential is stored across the 10 pF hold capacitor.
(3) Once the amplifier is disconnected, the stimulation signal can be applied to the electrode. In this phase, the stimulation circuitry is connected to the electrode (*stimulate* = *ON*) and both the *DAC data* and *polarity* control signals are updated every 50 μs, following the required shape of the stimulation pulse.
(4) After the stimulation pulse, the active discharging can be applied (*stimulate* = *OFF, discharge* = *ON, hold* = *OFF*). The duration of the discharging phase is defined in 50 μs time steps.
(5) After the discharging period, the amplifier is connected back to the electrode (*discharge* = *OFF, record* = *ON, hold* = *ON*) and recording is continued.

A simplified version of the protocol, including only disconnection of the recording amplifier, can be applied simultaneously to the non-stimulating channels. To achieve the maximum flexibility of the protocol, 12 bits of control data (7 amplitude bits, 1 polarity bit and 4 switch state bits) are updated in each sampling period and in each channel independently according to the external data stream.

To minimize the delay between the stimulation pulse and the start of the recording, one should not only optimize the shape of the stimulation pulse and the discharging duration time, but also minimize the delay between the end of the stimulation pulse and the start of the discharging period (steps 3–4) as well as between the end of discharging and the moment when the amplifier gets reconnected to the electrode (steps 4–5). In our design, the amplitude of the stimulation signal, as well as the states of the *stimulate, record, hold* and *discharge* switches, are refreshed synchronously with four separate trigger signals with appropriate delays to ensure non-overlapping switching of the switches in the channel. The triggers are generated in the chip based on a 5 MHz clock signal from the external controller, with relative timing set by the user with steps of 0.2 μs.

2.3. Stimchip architecture and control

The chip comprises 64 independent stimulation channels, programmable voltage and current bias generators, internal bandgap reference and control logic. The chip status is controlled by digital commands sent to the chip through the command line. A single command line can control independently up to 32 Stimchips. The commands are decoded by the logic block and the control signals are sent to logic circuits in selected channels. The channel logic controls the channel stimulation status (*enabled*/*disabled*), stimulation mode (*current* or *voltage*) and the range of the output signal (current or voltage depending on the stimulation mode). In addition, commands are used to define the relative timing of the internal trigger signals (see section 2.2). All these parameters must be defined prior to the experiment and cannot be changed in real time.

The stimulation waveforms and states of the artifact suppression circuits in all the active channels are controlled by a stream of real-time data received from an external PC through the 4 bit, 5 MHz data bus. To achieve a 50 μs period for refreshing the control data in all channels, 12 bits of information must be sent to each channel within this time frame. Using a 4 bit data bus, one has to send 192 words to load all 64 channels. The data are loaded into memory cells in the channels, and then, the states of the DACs are refreshed synchronously with an internal trigger generated by the on-chip logic block. Following this, the logic block generates triggers for refreshing the control signals (*stimulate*, *discharge*, *record* and *hold*) for the artifact suppression circuits. At a clock frequency of 5 MHz, one can execute the described protocol in 50 μs, with 38.4 μs used for transmitting the data and 11.6 μs for updating the parameters of the stimulation signals and the states of the switches in all channels. Within the 11.6 μs time window, the times to refresh the individual switches are defined by the user before the experiment in 0.2 μs steps (see section 2.2). For details of the real-time data protocol, see Hottowy *et al* (2008b).

The Stimchip has been designed and manufactured in the 0.35 μm, four-metal, two-poly CMOS process from Austria Microsystems. Since the ASIC architecture imposes cross-linking of the analogue and digital functionality in each

channel and across the whole chip, careful design of the mask layout was required to minimize injection of parasitic signals from the digital switching circuits to the high-precision analogue circuits. The mask layout has been designed using a full-custom technique, except for the logic block, which has been synthesized automatically. Particular attention has been paid to the symmetry of the layout and to the distribution of the power to ensure the best possible matching of parameters across the 64 channels (Hottowy *et al* 2008b). The chip power consumption is 30 mW when the stimulation is disabled on all channels and increases by 1.1–1.7 mW for each enabled channel depending on the defined stimulation mode and the range of the output signal. The modulation of power consumption by the specific stimulus shape is negligible.

A photo of the Stimchip is shown in figure 1(B). The total die area is 6400 $\times$ 2800 μm^2. The pitch of the input and output bonding pads is 100 μm so that the stimulation ASIC can be wire bonded directly to the recording ASIC (Grybos *et al* 2006).

2.4. Experimental setup

The Stimchip has been implemented in a setup based on a custom-made high-density MEA comprising 61 microelectrodes of 5 μm diameter, arranged in a hexagonal pattern with 60 μm interelectrode spacing (Litke 1999). The circular platinum return electrode is integrated with a plastic chamber that contains the neural tissue perfused with physiological solution (figure 1(D)). Prior to an experiment, the electrodes are routinely electroplated with platinum black for impedance reduction using the current generators of the Stimchip, which can be configured to deliver the electroplating dc current. Arrays of the same type have been used previously for the electrical stimulation of RGCs in rodents and primates (Sekirnjak *et al* 2006, 2008, 2009). However, those experiments were carried out using a stimulation/recording system based on an older stimulation integrated circuit (Platchip; see Dąbrowski *et al* 2004) with a functionality that is very much limited compared to the Stimchip.

The connections between the traces on the glass MEA substrate and the printed circuit board (PCB) are made with an elastomeric connector. Due to the geometry of the leads, two Stimchip ASICs are used for generation of the stimulation signals (figure 1(D)), with 32 channels of each Stimchip connected to the MEA; as the MEA includes 61 electrodes, three channels of the electronics are not used. The configuration commands and the stream of real time data for the chips are sent from a control PC equipped with a digital I/O card (National Instruments PCI-6534) and running a Labview application (the PC uses the standard 32-bit Windows XP operating system).

The neuronal signals from all the electrodes are recorded by two Neuroplat ASICs (Gryboś *et al* 2006), with each Neuroplat chip wire-bonded to a Stimchip (figure 1(E)). The Neuroplat ASIC comprises 64 independent ac-coupled recording channels with tunable gain and frequency pass band, and an analogue multiplexer. The available ranges of the recording channel parameters are 160–840 for the amplifier gain, 12–110 Hz for the lower cut-off frequency of the pass-band filter and 50–4500 Hz for the higher cut-off frequency. In addition, it is possible to set the input resistance value (within the range from 4 MΩ to 1 GΩ), which along with the coupling capacitor (190 pF) controls the cut-off frequency of the input ac-coupling stage. By changing the input resistance value and the lower cut-off frequency of the pass-band filter, it is possible to shape the noise characteristic of the recording channel (see Dąbrowski *et al* (2005) for details). In our experiments, the input resistance was set to 70 MΩ, which corresponds to an ac-coupling cut-off frequency of 12 Hz, and the pass band was set from 45 to 2000 Hz. The input-referred noise of the complete system, with these settings and with platinized electrodes immersed in a 0.9% NaCl solution, was 4.5–5 μV. We used gain values from 270 to 800, depending on the range of the stimulation currents used in a given experiment. The output signals from all the channels were sampled simultaneously with a frequency of 20 kHz, multiplexed and sent to the control PC for digitization and data storage. The digitization was carried out with a National Instruments PCI-6110 card equipped with 12-bit analogue-to-digital converters. The system design has been described in more detail by Hottowy *et al* (2008a).

2.5. Pilot experiments

2.5.1. Experimental procedure. In the pilot experiments, we stimulated and recorded from RGCs of adult mice and rats. Isolated pieces of retina were placed flat, ganglion cell layer down, on top of the array and superfused with oxygenated Ames' solution. The temperature of the bath was kept at 32 °C during the experiment (experimental details were the same as described by Sekirnjak *et al* (2006)). For the classification of the RGC types, we stimulated the photoreceptor layer of the retina with a flickering white-noise checkerboard visual image and simultaneously recorded the spiking activity of 30–40 RGCs in a single preparation (Litke *et al* 2004). The identification of the individual neurons and their corresponding spike times were carried out with custom-designed software in Java. As one example, in a rat retina preparation that provided the data described in subsections 3.3 and 3.4, 13 RGCs of type 'OFF-1' were identified. These cells are OFF cells with large visual receptive fields. (For the discussion on the functional classification of rat RGCs, see Anishchenko *et al* (2010).)

2.5.2. Electrical stimulation protocol. In all the experiments, we used a triphasic electrical stimulation signal waveform (positive–negative–positive sequence, as shown in figure 2) generated in the current mode. The relative amplitudes of the three phases were 2:–3:1 and the duration of each phase was set to 100 μs. In the following text, the term 'pulse amplitude' refers to the second (negative) phase of the pulse (for example, the pulse amplitude of 1.0 μA corresponds to the 0.67/–1.0/0.33 μA current phase sequence). All 61 electrodes of the array were routinely disconnected from the recording circuits for the duration of the pulse generated by any electrode to avoid saturation of the amplifiers. All the non-stimulating electrodes were reconnected to the amplifiers 5 μs after the end

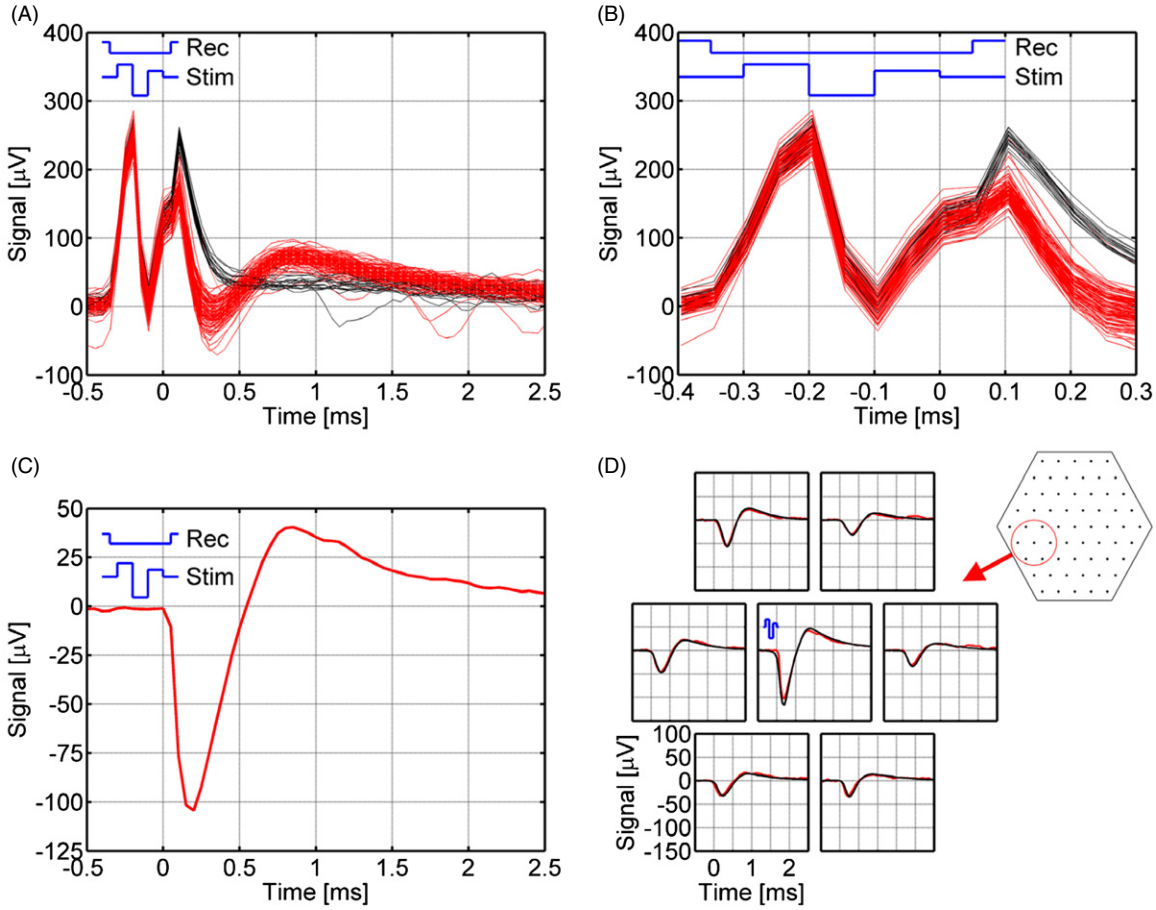

Figure 2. Low-artifact stimulation and recording of a single mouse RGC. (A) 100 responses to 0.43 μA stimulation pulses recorded on the stimulating electrode. The artifact-only responses are shown in black and the responses including spikes are shown in red. The stimulation current waveform and the state of the *record* switch disconnecting the electrode from the amplifier are shown in blue. (B) The same signals shown on an expanded time scale. The correlation between artifact shape and the stimulation current waveform is visible. (C) The averaged signal shape from the stimulated neuron shown after subtraction of the averaged artifact shape. (D) Comparison of the signals generated on the primary electrode and the six neighboring electrodes by the same neuron spiking under visual stimulation (black traces) and in response to the electrical stimulation (red traces, shown after artifact subtraction). The relative position of each plot in the figure follows the position of the corresponding electrode on the MEA layout. Both the vertical and the horizontal scales are the same for each plot. The 0.43 μA stimulation pulse was applied to the central electrode.

of the last phase of the stimulation waveform. In the case of the electrode used for stimulation, a delay of 55 μs was sufficient to obtain low artifact-related distortions and this value was used in all measurements.

2.5.3. Stimulation scan. To evaluate the responses of the RGCs to the electrical stimulation, we generated stimulation pulses on all the 61 electrodes, with currents ranging from 0.15 to 1.6 μA and with 10% amplitude increments. We always pulsed one electrode at a time, with 15 ms delay between pulses on consecutive electrodes. This delay between stimulation pulses was sufficient for the neural network response to return to a steady state after the stimulation. Within 1 s a single pulse was applied to each electrode. By repeating this procedure 100 times for each amplitude, in less than 45 min we recorded the responses of a population of RGCs as a function of the stimulating electrode location (61 electrodes) and current amplitude (26 values).

2.5.4. Analysis of stimulation efficacy. The response to the electrical stimulation of a given cell, with the cell identified as described in the subsection 2.5.1, was analyzed based on signals recorded for up to 2 ms after the beginning of the stimulation pulse. We analyzed the signals recorded by the electrode that showed the largest signal recorded from this neuron (named the 'primary recording electrode') and the six neighboring electrodes. To separate the signals coming from possibly several neurons plus the stimulation artifacts, the spike waveforms from the primary electrode and the neighboring electrodes were projected onto principal component analysis (PCA) space and classified manually based on the three most significant PCA variables. The stimulation efficacy was defined as the probability of initiating an action potential in a cell stimulated by a specific electrode. The experimental data of efficacy ε versus the stimulation current I was fit to the sigmoidal function $\varepsilon = 1/(1 + \exp(-aI + b))$. The stimulation current threshold was then defined from this fit as the current necessary for the stimulation of the given cell with an efficacy of 50%. The 'primary

stimulation electrode' for the given cell was the electrode that provided the lowest stimulation threshold for this cell.

2.5.5. Stimulation with spatio-temporal patterns. In one experiment, we aimed at the replication of the light-evoked activity in the population of 13 'OFF-1' RGCs that were described in subsection 2.5.1. Based on the results of the stimulation scan, we identified online the primary stimulation electrodes and the stimulation thresholds for 10 out of the 13 'OFF-1' cells identified in this preparation. (We note that the offline analysis performed after completion of the experiment indicated that 12 'OFF-1' cells were effectively stimulated during the scan. The 13th cell was not stimulated by currents up to the maximum value of 1.6 μA employed in the scan.) To replicate the visually evoked spiking activity generated by a single RGC, we defined a sequence of stimulation pulses that matched the time series of action potentials recorded previously as this RGC was stimulated with a 1 s long spatio-temporal white noise visual stimulus. The current pulses were generated on the primary stimulation electrode of this cell, with the minimal amplitude necessary to stimulate the cell with 100% efficacy.

To replicate the activity of the population of RGCs, we combined the pulse sequences for each of the ten OFF-1 cells into one spatio-temporal pattern of stimulation pulses. All 61 electrodes were routinely disconnected from the recording amplifiers synchronously with the stimulation pulse generated on any of the electrodes. All the pulse timings were binned with a step of 2 ms to ensure that the recording following the stimulation pulse on one electrode was not disturbed by the stimulation pulse on another electrode.

Since the sensitivity of the RGCs to an electrical stimulation can be reduced for a high-frequency stimulation (Sekirnjak *et al* 2006), the stimulation pulses were generated with an additional scaling of the pulse amplitudes. All the amplitudes were multiplied by the same factor, incremented from 0.8 to 2.0 with a 10% increase for each consecutive step. For each scaling factor value, we applied the complete pattern of stimulation pulses 20 times with a repetition period of 3 s. The complete procedure took ~11 min.

After the recording, we suppressed the spiking activity by adding the sodium channel blocker TTX (1 μM) to the perfusion solution and repeated the stimulation protocol to record the stimulation artifacts. These artifacts were subtracted from the original data in the offline analysis to reconstruct the RGC responses to the stimulation pulses (Sekirnjak *et al* 2006).

To estimate the timing of an evoked spike with respect to the stimulation pulse, we used the recorded response on the primary recording electrode after artifact subtraction (as explained above). Since the first (negative-going) edge of the neuronal spike can be slightly distorted by the artifact, we used the second (rising) edge of the (negative) spike waveform to estimate the spike times. For each spike, we found the time when this spike edge crossed the level equal to one-half of the negative spike amplitude, and this time minus the average spike width at the half-amplitude (estimated based on light-evoked activity of this cell) was defined as the spike latency. It should be noted that while in engineering papers the stimulation response time is typically defined in reference to the end of the stimulation pulse—as in this study—some neuroscientists prefer to define the latency in reference to the pulse onset (Sekirnjak *et al* 2006). For a direct comparison of our results with some studies, the spike latencies reported here must be increased by the value of pulse duration (300 μs).

The latency uncertainty was calculated as the standard deviation of the spike time distribution.

3. Results

3.1. Low-artifact stimulation of individual neurons

Figure 2(A) shows 100 overlaid responses of a mouse RGC to 0.43 μA stimulation pulses, recorded on the stimulating electrode. One can easily notice two classes of recorded waveforms. We classified 86 of the recorded waveforms as the superposition of stimulation artifacts and the elicited neuronal spikes (red traces) and 14 waveforms as the artifacts only (black traces).

The three-phase stimulation pulse was initiated at $t = -0.3$ ms and terminated at $t = 0.0$ ms. The amplifier input was disconnected from the stimulating electrode for the period from $t = -0.35$ ms to $t = 0.05$ ms for each stimulation waveform, and the artifacts recorded during that period (figure 2(B)) are due to crosstalk between the electrode and the amplifier input through the parasitic capacitances of the open CMOS switch (the *record* switch in figure 1(A)). The optimized shape of the stimulation current waveform results in a minimal residual charge left on the electrode–electrolyte interface and we observe only a low-amplitude artifact after reconnecting the amplifier input to the electrode.

The amplitudes of the recorded artifacts are within the same range as the typical amplitudes of the neuronal spikes and well within the amplifier linear range (± 1 mV input signal for the gain set to 800). Thus, we can assume that the system can recover the elicited spikes, after artifact subtraction, with a quality similar to that of the spontaneously generated spikes. To verify this, we averaged the waveforms within each of the two classes shown in figure 2(A) and subtracted the obtained average waveforms to find the average shape of the recorded elicited spikes (figure 2(C)). The same procedure was applied also to the electrodes adjacent to the one used for the stimulation. As shown in figure 2(D), the averaged elicited spikes match very well the averaged spikes generated by the same neuron spiking spontaneously. Therefore, with a simple artifact subtraction, it is possible to reconstruct the shapes of the elicited spikes with minimal distortion, even on the electrodes used for the stimulation and for spikes with latencies as short as ~0.1 ms relative to the end of the stimulation pulse.

The method presented for spike-shape reconstruction requires that the signals recorded after the stimulation pulse, which are combinations of stimulus artifacts and neuronal responses, do not exceed the linear range of the recording circuitry. As the artifact level changes with the stimulation amplitude, this requirement may not be met for larger stimulation amplitudes. Based on results of the stimulation

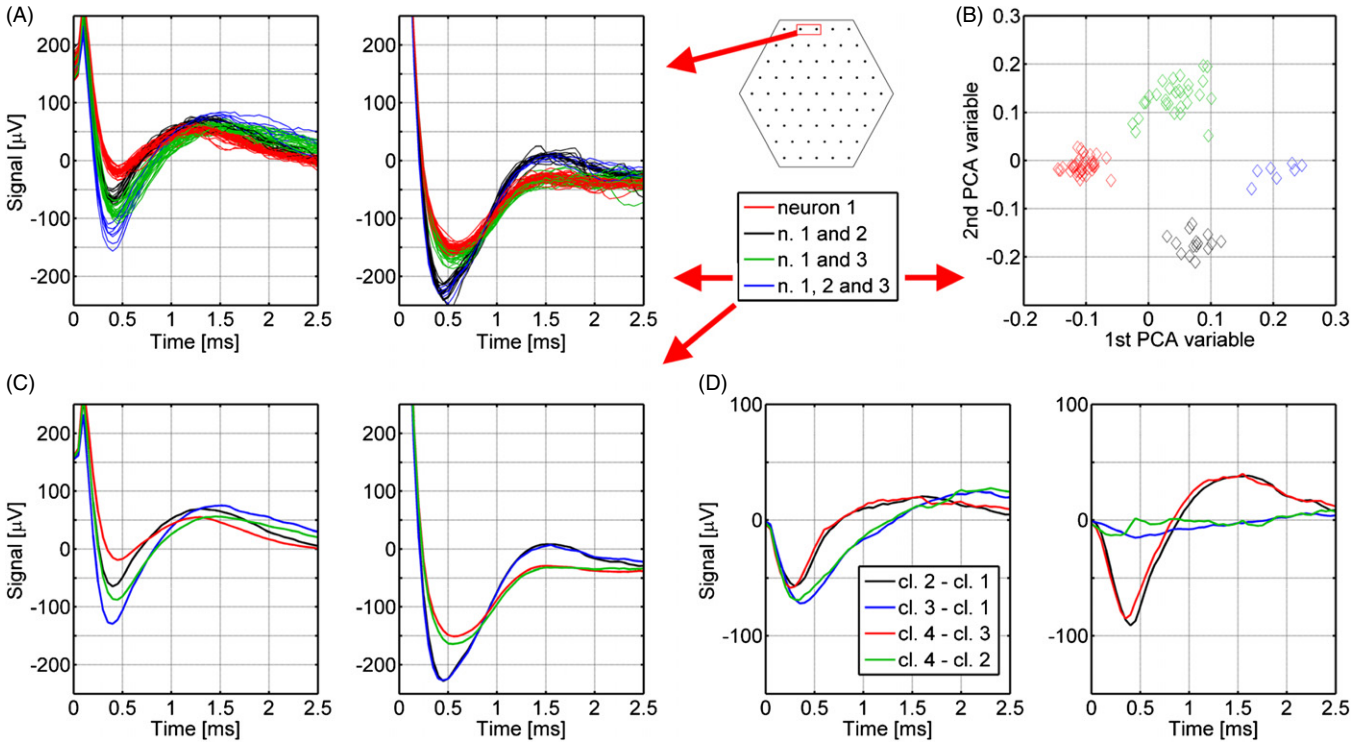

Figure 3. Detection and identification of signals from simultaneously stimulated neurons in the mouse retina. (A) 98 responses to 0.65 μA stimulation pulses recorded on the stimulating electrode (left panel) and one of the neighboring electrodes (right panel). The vertical scale range is the same for both panels. The four color-coded clusters of the recorded responses originate from the combined activity of three stimulated neurons (see the text). The MEA layout indicates the location of the stimulating electrode (on the left) and the neighboring electrode. The legend box shows the color code, in A, B and C, for the four response combinations of the three neurons. (B) Scatter plot showing the four color-coded clusters based on the two most significant PCA variables derived from the spike waveforms shown in A. (C) Averaged waveform shapes for the four clusters of recorded responses shown in (A). (D) Reconstructed shapes of the signals recorded from neurons 2 and 3 on the two electrodes, based on the average waveforms shown in (C) (see the text).

scan procedure (section 2.5.3), we analyzed for each channel the responses to stimulation pulses generated on the given channel. For the stimulation amplitudes up to 1.6 μA and the gain of the amplifiers set to 270, only three channels show saturation following the stimulation pulse. The remaining 58 channels (>95%) were able to start recording of neuronal responses immediately after they were connected back to the electrode.

3.2. Multineuron stimulation with a single electrode

By increasing the amplitude of the stimulation current, we could stimulate several neurons with the same electrode. In such a case, the responses to the stimulation pulses can include different combinations of spikes from these cells. In figure 3(A), we show overlaid responses (recorded on the stimulating electrode and one of the neighboring sites) to 0.65 μA stimulation pulses that activated three independent mouse RGCs (#1–3) with efficacies of 100%, 23% and 38%, respectively (the stimulus was repeated only 98 times in this experiment). The signal from neuron #1 contributes equally to each of the displayed responses and it cannot be separated from the stimulus artifact—we identified this neuron based on the analysis of responses to lower stimulation amplitudes (data not shown).

The displayed waveforms split well into four separate clusters in the PCA space (figure 3(B)), based on the correlated waveforms recorded on the two indicated electrodes. We associate the four PCA clusters with the following groups of signals: (1) the artifact combined with the signals from neuron #1—45 red traces; (2) the artifact superimposed with the signals from neurons #1 and #2—16 black traces; (3) the artifact and the signals from neurons #1 and #3—30 green traces; and (4) the artifact combined with signals from neurons #1, #2 and #3—7 blue traces. The average signal waveforms associated with each cluster, on each of the two electrodes, are shown in figure 3(C).

The average signal shape for neuron #2 can be estimated as the difference between the averaged waveforms associated with clusters (2) and (1), or as the difference between the waveforms for clusters (4) and (3). Similarly, the signal shape for neuron #3 can be obtained either by subtracting cluster (1) from cluster (3) or cluster (2) from cluster (4). The estimated signal shapes are shown in figure 3(D). One can see that for both neurons #2 and #3 the two estimation methods give nearly identical results, which confirms our hypothesis regarding the origins of the recorded signals. These results indicate that at least in some cases the signal recorded from multiple neurons spiking simultaneously is a linear superposition of the signals generated by these neurons and that the low-artifact stimulation provided by the Stimchip allows for proper identification of the responses from individual stimulated neurons, even if more than one cell is activated with the same electrode and stimulation amplitude.

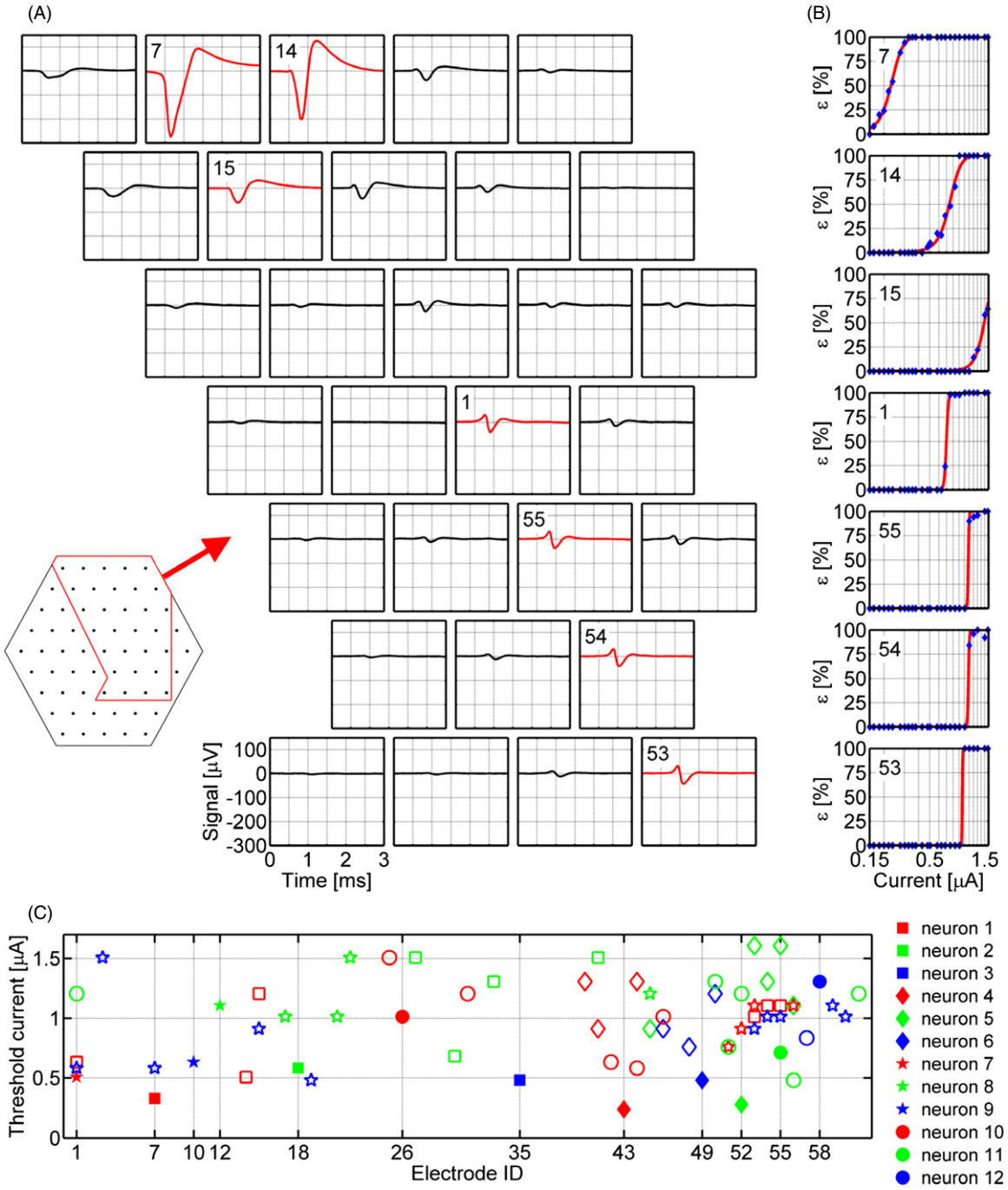

Figure 4. Sensitivity of a rat RGC to the stimulation applied to various electrodes. (A) The EI for neuron #1 (as labeled in the legend for (C)), based on the averaged waveforms recorded from the cell on 30 electrodes during the visual stimulation. The red traces mark the seven electrodes (labeled with the electrode IDs as in (C)) that activated the cell during the electrical stimulation with currents ranging from 0.15 to 1.6 μA. The relative position of each plot in the figure follows the position of the corresponding electrode on the MEA layout. (B) Stimulation efficacy as a function of the stimulation current for the seven indicated electrodes. The blue diamonds show the experimental results and the red curves show the fits with a sigmoidal function. (C) The threshold currents, for 100% and 10% stimulation efficacies, as a function of electrode number for 12 'OFF-1' RGCs in a single retina. The symbols mark the minimal currents needed for the stimulation of a given cell with 100% efficacy (full symbols—shown for the 'primary stimulation' electrode for each cell) or 10% efficacy (open symbols).

3.3. Spatial map of stimulation threshold

We used the automated 'scan' procedure (section 2.5) to find how RGCs in the rat retina responded to stimulation pulses applied to various electrodes with different amplitudes. Typical results for one specific type of RGC are shown in figure 4. These RGCs are of type 'OFF-1' as has been described in subsection 2.5.1.

Figure 4(A) shows the 'electrophysiological image' (EI) (Litke *et al* 2004) of an individual OFF-1 cell, based on the average spike waveforms recorded from this RGC, during visual stimulation, on the 30 indicated electrodes, including

the 7 electrodes that effectively electrically stimulated the cell. Three of these electrodes (labeled 7, 14 and 15) recorded the biphasic somatic signals and the four remaining electrodes (1 and 53–55) recorded the triphasic, propagating axonal signals of the cell (Litke *et al* 2004).

The stimulation efficacies as a function of the current amplitudes are shown in figure 4(B) for each of the seven electrodes. The non-local, axonal stimulation by electrodes 1 and 53–55 are examples of an antidromic stimulation whereby the stimulation of the neuron's axon is followed by backward propagation of the evoked impulse toward the soma and subsequent action potential generation by the cell. The efficacy curves in this case are very steep, with the response rate switching from 0% to 100% for a current increase of about 10%, while for the cell body stimulation (electrodes 7, 14, 15) the efficacy versus the amplitude dependence is much more gradual (this effect was typical for all analyzed cells). This cell was stimulated with the lowest threshold by electrode #7 that also recorded the largest signal from this neuron. When stimulating with this electrode, the initiation of an action potential with a probability of 50% required a current of 0.25 μA, while for all the other electrodes the required current value was at least 0.7 μA.

For the 13 'OFF-1' RGCs identified in this preparation, based on the white noise visual stimulation procedure (subsection 2.5.1), 12 cells were effectively stimulated by at least one electrode. (As noted in section 2.5.5, the 13th cell could not be stimulated by currents as high as 1.6 μA, the highest current employed in the scan.) For 10 of these cells the primary recording electrode, which always indicated a cell body signal, was the same as the primary stimulating electrode (section 2.5.4), consistent with the example shown in figure 4(A). For the two remaining cells, one was stimulated most effectively with an electrode recording a somatic signal and adjacent to the primary recording electrode. For the other cell, the soma was located near the array corner (probably outside the active MEA area) and this neuron was stimulated most effectively with an electrode located close to its axon.

In figure 4(C), we show the distribution of the stimulation thresholds for the 12 cells and the 61 electrodes of the MEA. The minimal stimulation amplitudes required for the stimulation of a given cell with 100% efficacy, using the 'primary stimulation electrode' for this cell, are shown with full symbols. The minimal stimulation current, leading to activation of a cell with an efficacy of 10% or more, was marked with an open symbol at the corresponding electrode ID. By inspection of the plot, one can identify for each of these RGCs an electrode and stimulation amplitude which provides the stimulation of the given RGC with 100% efficacy without stimulating activity in the other identified cells of the same type.

One should note the following factors that made an independent stimulation of individual RGCs within the 'OFF-1' population possible, namely (1) the 'OFF-1' RGCs form a mosaic (Field and Chichilnisky 2007) thereby providing spacing ($\sim$100–150 μm) between the RGC cell bodies, (2) the interelectrode spacing of the MEA is 60 μm, approximately one-half of the 'OFF-1' spacing, (3) by stimulating a specific RGC with an electrode located in the vicinity of the cell body, one gets a significantly lower stimulation threshold than for different electrode locations and (4) the Stimchip can provide independent stimulation pulses, with tunable current amplitudes, to each electrode. These conditions make possible an independent stimulation of the individual cells. However, there remain three important related issues that will be discussed in section 4.4: (1) the independent stimulation of RGCs of different cell types, (2) non-local axonal stimulation and (3) optimization of the stimulation currents, taking account of changes in thresholds due to recent past stimulations and/or spiking activity.

3.4. Stimulation with spatiotemporal patterns

According to the results presented in subsection 3.3 and shown in figure 4(C), for 12 of the 13 identified 'OFF-1' RGCs the primary stimulation electrode can stimulate a given neuron at a current level that makes simultaneous activation of the other 'OFF-1' cells unlikely. This suggests that it should be possible to independently stimulate individual 'OFF-1' RGCs and finally to generate a precisely defined sequence of spikes in a population of these neurons.

To verify this, we first measured the spiking activity, evoked by 1 s of white noise visual stimulus, in the population of 'OFF-1' RGCs. We then defined a spatio-temporal pattern of electrical stimulation pulses to replicate this activity in ten of these cells and applied this stimulation pattern through the corresponding primary stimulation electrodes. The ten cells included in the patterned stimulation are the same cells as in figure 4(C), except for neurons #7 and #9 for which the stimulation thresholds were not identified during the online analysis. (These thresholds were identified offline after the experiment; see subsection 2.5.5).

The complete pattern included 208 stimulation pulses distributed over the ten electrodes during 1 s. This pattern was repeated 20 times with a period of 3 s for each value of the scaling factor (see subsection 2.5.5). The best compromise between an efficient activation of the targeted cells and the avoidance of activation of non-targeted cells within the population of 'OFF-1' RGCs was obtained for the scaling factor value of 1.56. For seven of the stimulated neurons, we found the desired response: each of these cells was reliably activated by its primary stimulating electrode and showed no activity synchronized with the stimulation pulses applied to any of the other electrodes (these were neurons 2, 3, 4, 5, 6, 10 and 11, as indicated in figure 4(C)). The eighth cell was clearly activated by both its primary stimulation electrode and one of the other nine electrodes. This RGC is indicated as neuron #1 in figure 4(C); this is the same neuron that is shown in figures 4(A) and (B). Finally, for the two remaining cells (8 and 12), the results of the crosstalk analysis were not clear. We noted that the current pulses generated at two of the ten stimulating electrodes initiated large, axon-like signals recorded on many electrodes of the MEA (data not shown). The analysis of the spatial distribution of these signals suggests that they were associated with the stimulation of axonal bundles; however, more analysis is needed to understand

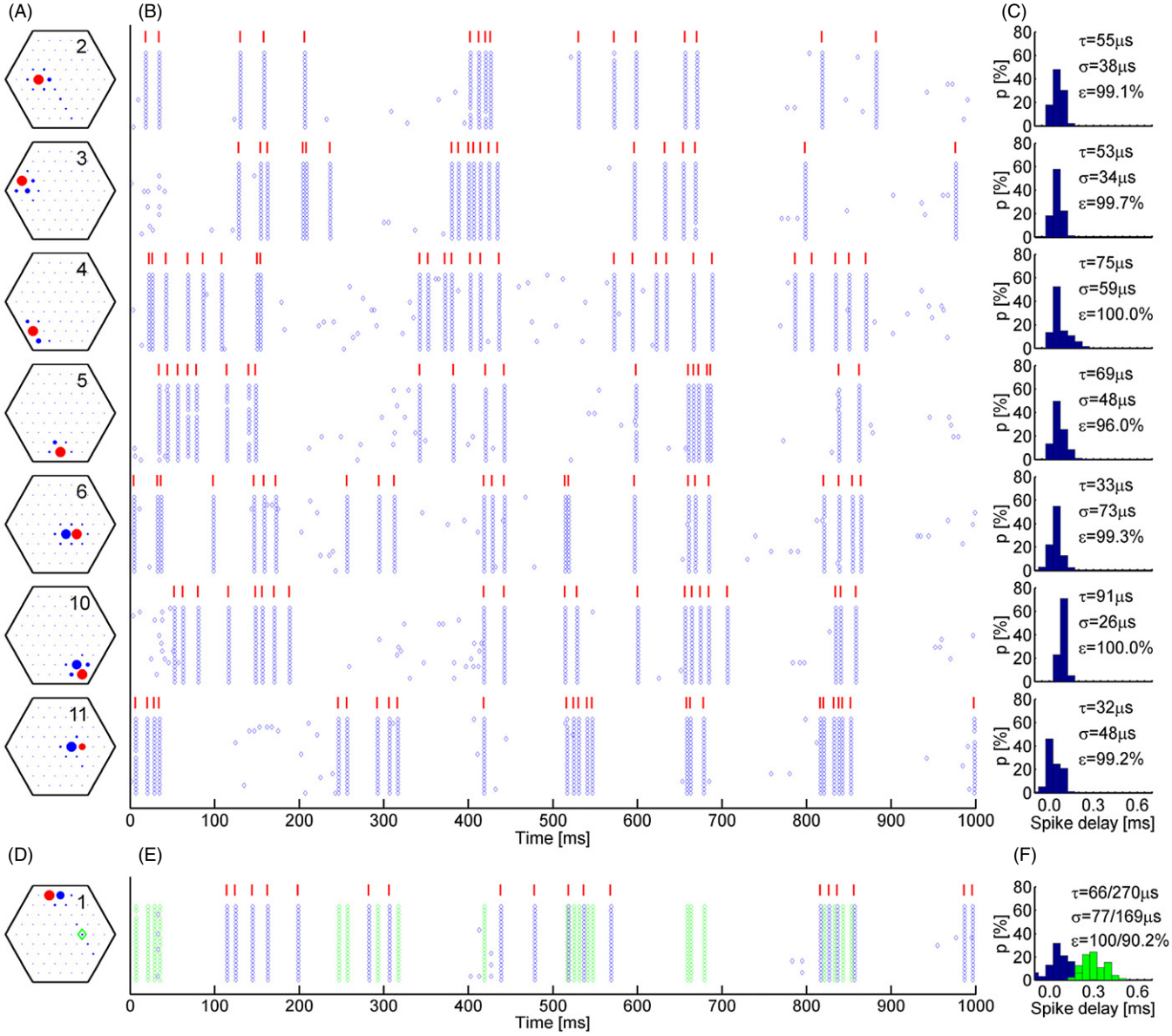

Figure 5. Replication, in an isolated rat retina, of the visual stimulus-evoked spiking activity of a RGC population with the patterned electrical stimulation. (A) Averaged recorded visually evoked signal amplitudes of seven 'OFF-1' RGCs, shown on all 61 electrodes (EIs). The circle diameter is proportional to the average amplitude and the circle center corresponds to the position of the given recording electrode. The red circle marks the electrode that was used for the electrical stimulation of the given cell. The number in the upper right corner of the array marks the neuron ID, as indicated in figure 4(C). (B) RGC responses to the patterned electrical stimulation. For each cell, the red lines mark the stimulation pulse times and the blue diamonds mark the spike times. The spike times are presented in 20 rows that correspond to 20 repetitions of the 1 s electrical stimulation pattern. The stimulation amplitude was adjusted for each cell independently. (C) Distributions of spike delays relative to the end of the stimulation pulse; τ—average delay; σ—variability (SD) of neuron response delay; ε—stimulation efficacy; p—probability of response within 2 ms after the stimulation pulse. (D), (E), (F) EI, stimulation response and spike delay distribution for one RGC (neuron #1, as labeled in figure 4(C)) that was stimulated by both its primary electrode (#7) and another electrode (#55), as shown in figure 4(A). The electrode (#55) generating the crosstalk (D), the spikes resulting from the crosstalk (E) and the distribution of these spike delays relative to the stimulation by this electrode (F) is marked with the green color.

this phenomenon completely. Since these signals were also detected at the primary recording electrodes for neurons 8 and 12 and they could potentially mask the action potentials from these cells, making the analysis of the crosstalk for these cells problematic, we excluded these neurons from further analysis.

The EIs of the seven cells are shown in figure 5(A); the red dot indicates the electrode used for the stimulation of the given cell. The corresponding stimulation pulse times are shown as red lines in figure 5(B). The 20 responses of each of the seven neurons to the 20 applied sequences of stimulation pulses are shown as blue diamonds in the same figure. The neuron spiking activity follows the applied stimulus sequences with excellent reproducibility, with an efficacy of ∼99%, an average spike latency of ∼50 μs and a spread of the spike latency (SD) of ∼50 μs (see figure 5(C)). We conclude that with a careful optimization of the stimulation pulse amplitudes, the Stimchip-

based system can generate a complex, precisely defined pattern of activity in a population of selected RGCs.

In figure 5(D), we show the EI of the eighth OFF-1 RGC (neuron #1 in figure 4(C)) that responded well to the stimulation on its primary stimulation electrode (#7, indicated by the red dot) but was also antidromically activated by electrode #55 (indicated by the green diamond) that was located close to the cell's axon, as shown in figure 4(A). The axonal stimulation of neuron #1 has, as a consequence, crosstalk in the patterned stimulation. We see in figure 5(E) that in addition to the desired spiking responses of neuron #1 (blue diamonds) by electrode #7 (red lines), mimicking the visually evoked activity, there are extra (undesired) responses (green diamonds) due to crosstalk from the stimulation of neuron #11 by electrode #55 (red lines for the bottom cell in figure 5(B)). Figure 5(F) shows the spike latency distributions for the primary (blue) and axonal (green) stimulations.

In addition, we analyzed the responses to the pattern stimulation of the 15 RGCs of other than 'OFF-1' types identified in this preparation. We found an antidromic axonal stimulation in two of these cells and a somatic stimulation in three cells. As none of these 15 cells were targeted for the stimulation, all these responses must be considered as crosstalk effects.

4. Discussion

4.1. Stimchip functionality and compatibility

In table 1, we compare the functionality and performance of the Stimchip with other reported stimulators designed for MEA-based two-way electrical communication with neural networks. Compared with these designs, the Stimchip allows for the generation of much more complex stimulation patterns than any other system. The chip generates 64 independent stimulation signals, while the other reported systems allow for the generation of one to eight independent signals. Furthermore, thanks to the VLSI technology used for the design of the stimulator, it is possible to build a compact system comprising many Stimchips working in parallel and providing independent stimulation signals to hundreds of electrodes on a large-scale MEA. Indeed, we have developed a completely functional 512-electrode MEA system with 512 independent stimulation and recording channels. For a description of this system and preliminary test results with retinal and cultured brain slice preparations, see Hottowy *et al* (2010).

An important feature of the Stimchip is its compatibility with various applications and MEA designs. This implies the ability to generate the stimulation signals over a wide range of current and voltage amplitudes. For example, an extracellular stimulation of individual cells typically requires current amplitudes of the order of microamps (Sekirnjak *et al* 2006, Houweling and Brecht 2008), but values as low as 40 nA have been reported for specific electrode–neuron configurations (Buitenweg *et al* 2002). On the other hand, for eliciting behavioral responses, the stimulation amplitudes of several hundred microamps may be necessary (Tehovnik 1996). In addition, some researchers prefer generation of the stimulation signals in a voltage mode. In such a case, the injected current amplitude and waveform are difficult to control, as the impedance of the electrode–electrolyte interface can vary from electrode to electrode, but direct control of the electrode voltage helps avoid water electrolysis, which can be dangerous for the tissue (Merrill *et al* 2005). Therefore, the final choice between the current and the voltage stimulation modes depends on the priorities of the specific experiment.

The integrated circuit presented in this paper can generate stimulation signals in both the current and the voltage mode, with amplitudes ranging from 0.5 nA to 1 mA and from 12 μV to 1.5 V, respectively. The total dynamic range in the current stimulation mode is equal to 22 bits, including 8 bits controlled in real time by switching the DAC value and polarity, and an additional 14 bits of variable gain in the output buffers. In the voltage mode, the dynamic range is equal to 18 bits (8 + 10). These ranges are sufficient for a wide range of experiments based on the electrical stimulation; however, the maximum output voltage of 1.5 V (which applies to both the current and the voltage mode) can be a limiting factor in some applications.

The Stimchip's ability to generate current signals with extremely low amplitudes (down to 0.5 nA peak-to-peak) and arbitrary waveform shapes opens the possibility for fast measurement of the electrode impedance as a function of frequency. Since the Neuroplat chip can record signals with amplitudes up to 10 mV peak-to-peak (for minimum available gain = 160), the measurement of impedances up to 20 MΩ is feasible. Such measurement can be used to estimate the range of stimulation currents available in each channel without exceeding the maximum output voltage of the Stimchip circuitry. Since the impedance of the electrode–electrolyte interface decreases in general with an increase of the cross-interface voltage (McAdams *et al* 1995), the estimation of the maximum available current based on the impedance measured with low currents would be in fact fairly conservative. Based on the impedance model for the microelectrodes used in this study (Mathieson *et al* 2004), we estimate the maximum amplitude for the triphasic pulse (2:–3:1 relative amplitudes, 100 μs duration per phase) in our system to be on the level of 11 μA.

It should be noted that the implementation of the real-time control of the stimulation signal waveform and artifact cancellation circuitry in each channel, although offering uncompromised flexibility of the stimulation protocol requires a massive data stream of $\sim$15 Mb s^{-1} from the off-chip controller. Although this data transmission rate is not a problem for most applications, the chip design may not be optimal for a bandwidth-limited application, such as a wireless system. In such a case, predefinition of the stimulation current waveform (presumably for each channel independently) combined with real-time transmission of trigger signals could be a more appropriate solution.

4.2. Low-artifact stimulation

Another advantage of the Stimchip, compared with other reported systems, is its ability to provide an electrical stimulation with exceptionally low artifacts (see table 1). In our design, the artifact minimization protocol is controlled

Table 1. Comparison of the functionality and performance of the Stimchip-based system and other MEA systems for two-way communication with neuronal networks.

Reference	Technology of stimulation/recording electronics	Number of stimulation channels	Number of independent stimulation signal sources	Electrode diameter/ spacing (μm)	Application	Artifact duration on stimulating electrode/adjacent electrode (ms)
Jimbo *et al* (2003)	Discrete elements	64 voltage	1 external	10–50/50–250	Rat cortex	>2/not reported
Wagenaar and Potter (2004)	Discrete elements	64 current or voltage	1 internal (8 bit)	30/200	Rat cortex	>40/>1
Sekirnjak *et al* (2006, 2008)	CMOS	64 current	1 external	5/60	Rodent and primate RGCs	5/0.05
Heer *et al* (2007)	CMOS (MEA integrated on chip)	128 voltage	1 internal (8-bit)	30/250	Rat hippocampus	>2/>1
Brown *et al* (2008)	CMOS	16 voltage	1 external	40/200	Hippocampus (mouse or rat)	3/0.5
Rolston *et al* (2009)	discrete elements	64 current	1 external	33/175	Rat hippocampus	5/0.4
Frey *et al* (2010)	CMOS (MEA integrated on chip)	126 voltage	2 internal (10 bit)	7/18	Not reported	>10/>50
Charvet *et al* (2010)	CMOS	256 current	8 external	Various	Mouse hindbrain	Not reported
This work	CMOS	64 current or voltage	64 internal (8 bit)	5/60	Rodent RGCs	0.055/0.005

independently for each channel, with a high temporal resolution, whether or not the given channel generates the stimulation current. This flexibility, combined with an optimized shape of the stimulation pulse, allows for very efficient artifact minimization. In our experiments, we were able to record the neuronal responses as soon as 55 μs after the stimulation pulse on the stimulating channel and almost immediately (5 μs after the pulse) on the other channels. In comparison, the other reported systems cannot record neuronal responses for at least 2 ms on the stimulating channel and 0.4 ms on the other electrodes (table 1). One exception is the system used for the stimulation of RGCs (Sekirnjak *et al* 2006, 2008, 2009) that allowed for detection of some of the neuronal responses on non-stimulating electrodes with delays similar to those reported in our study. However, using a microelectrode array identical to ours, they were able to identify responses from only 5–7 cells in a single preparation, while our system allowed for recording of the elicited activity from virtually each cell targeted for the stimulation (see sections 3.1 and 3.3) including signals from the stimulating electrode. In the context of data presented in figure 2, we conclude that the Stimchip-based system presented here offers very significant improvement in the quality of recording of neuronal responses to the electrical stimulation, especially in the case of low-latency responses from directly activated cells.

We emphasize the necessity of reduction of both the artifact level recorded during the stimulation pulse and the post-stimulus artifact related to charge accumulation at the double layer of the stimulating electrode. The electrode voltage waveform during the stimulation pulse can be very large compared to the amplitudes of the recorded spikes and the linear input range of the recording circuitry—specifically at the stimulating electrode, for which the electrode voltage is practically limited by the output voltage limit of the stimulation circuitry. Significant reduction of this part of the artifact is critical to avoid saturation of the recording amplifier, as the recovery of the recording circuitry may take up to hundreds of milliseconds (for discussion see Jochum *et al* (2009)) making detection of the neuronal response to the stimulation impossible. This requires careful scaling of the transistors forming the blanking switch (the *record* switch in figure 1(A)). These transistors need to have very high impedance in the open state to assure low crosstalk of the input artifact to the input resistance of the amplifier and, at the same time, must provide low-resistance connectivity in the closed state (preferably, much lower than the spread resistance of the electrode) to avoid a noticeable noise contribution during recording. In our design, the resistance of the record switch in the closed state is $\sim$1 kΩ, reasonably low compared to $\sim$60 kΩ spread resistance of our microelectrodes, or even $\sim$10 kΩ of spread resistance in the case of larger electrodes with a diameter of 30 μm. We also note that we did not notice any saturation problems caused by the crosstalk-related artifact during our experiments.

By comparison of the modeled electrode voltage during the stimulation pulse, predicted using the linear electrode impedance model of Mathieson *et al* (2004), with the amplitude of the artifact visible in our data during the pulse on the stimulating channel, we conclude that use of the *record* switch allowed us to reduce the artifact level by a factor of approximately 200. This artifact reduction factor was fairly constant for the current values used in our scan procedure (0.1–1.6 μA). This constancy is an expected result, as both the impedance of the open CMOS switch and the input resistance of the Neuroplat chip—the two impedances that form the voltage divider for the electrode voltage waveform—are independent of the electrode voltage. For the maximum output voltage of the Stimchip stimulation circuitry ($\pm$1.5 V), the amplitude of the artifact resulting from the crosstalk effect should not exceed $\pm$7.5 mV. In comparison, the linear input range of the Neuroplat chip with the gain set to 160 (lowest available setting) is $\pm$5 mV. However, it should be noted that the artifact reduction factor is expected to be a function of the input resistance of the recording amplifier and, due to the capacitive impedance of the open *record* switch,

also of the shape and duration of the stimulation pulse. With the ability to control the stimulation waveform as well as the amplifier gain and the input resistance of our system, it should be possible to avoid the crosstalk-related saturation effect even for larger stimulation amplitudes and for different electrode designs from that used in our study.

The problem of the reduction of the post-stimulus artifact is unique to the stimulating electrode. Due to the complex impedance of the electrodes, the stimulation pulse results in charge accumulation at the electrode surface that in turn leads to an artifact visible in the recordings after the stimulation pulse is finished and the recording amplifier is reconnected to the electrode. We note the importance of an optimized stimulation pulse shape for the effective minimization of this part of the stimulation artifact. For example, the detection of short-latency neuronal responses in our experiments was not possible when we used a standard biphasic stimulation pulse followed by active discharging of the electrode–electrolyte interface (data not shown). The short latency of the elicited responses allows only a very short time for the discharge, of the order of 100 μs, while significant artifact reduction requires an active discharging time on the order of milliseconds (Jimbo *et al* 2003, Brown *et al* 2008). Since the time constant of the discharging process is determined by the impedance of the electrode–electrolyte interface and the spread resistance of the extracellular medium, it is very difficult to shorten this time for a given electrode technology and stimulation amplitude. However, by adding an additional phase to the stimulation waveform, as in the experiments discussed in this paper, the charge required for significant reduction of the electrode resting potential can be injected quickly. In our experiments, such a triphasic stimulation pulse allowed us to record the neuronal responses at the stimulating electrodes without any post-stimulus saturation problems on $>$ 95% of the channels (see section 3.1). However, even if the shape used in this study allowed us to record the responses from RGCs with very low distortions, the generalization of this method to other systems and applications will require more systematic studies, including modeling of the artifact phenomena based on realistic models of the electrode–electrolyte interface impedance. For best results, the pulse shape should be optimized for the specific electrode design and stimulation amplitude. The optimization procedure should also take into account the intrinsic delay of the neuronal response to an electrical pulse, which limits the acceptable latency between the stimulation pulse and the time for signal recording recovery. It should be noted that the results presented here do not allow the precise identification of the moment when the membrane depolarization exceeds the threshold for action potential initiation. It is then difficult to predict, based on these data, the timing of the stimulated action potential in relation to the stimulation pulse for different pulse shapes and durations. Thus, despite minimal delays between the end of the stimulation pulse and the beginning of the response recording reported in this study, the fact that the recording functionality is turned off during the pulse duration can in principle be limiting. For example, if the action potentials were generated by the first pulse phase, our recording would effectively start $\sim$200 μs after the pulse initiation (at the non-stimulating electrode, assuming 100 μs per phase duration). One of the interesting future applications of the system presented here would be to investigate the dynamics of neuronal responses to the electrical stimulation by examination of the effects of different waveform types, including triphasic pulses of different polarities (cathodal–anodal–cathodal versus anodal–cathodal–anodal sequences).

4.3. Stimulation of individual RGCs

The stimulation current thresholds for direct activation of individual ganglion cells presented in section 3.3 are consistent with published results from similar experiments (Jensen *et al* 2003, Sekirnjak *et al* 2006). Our result on the specifically high sensitivity of RGCs to stimulation currents injected in the vicinity of the cell body (see section 3.3) was also reported before (Jensen *et al* 2003, Sekirnjak *et al* 2008) and attributed to the very high density of the sodium channels in the proximal axon region (Fried *et al* 2009). To our knowledge, our observation on the steeper efficacy–stimulation current curve for the axonal stimulation, compared to the stimulation of the cell body, has not been previously reported.

4.4. Stimulation of a population of RGCs

Our result on the replication of the spatio-temporal spiking activity in a population of neurons is new in the literature. It was shown previously that the epiretinal stimulation with microelectrodes can initiate action potentials in individual RGCs with high reliability and temporal precision, even at high stimulation frequencies (Fried *et al* 2006, Sekirnjak *et al* 2006). Fried *et al* (2006) used relatively large electrodes ($>$5000 μm^2) and stimulation currents ($>$100 μA) to replicate a light-evoked activity in RGCs, but the issue of an independent stimulation of individual cells was not addressed. Sekirnjak *et al* (2008) used a microelectrode array identical to ours to selectively activate individual Parasol-ON and Parasol-OFF cells in the primate retina, with an independent stimulation of even the closest-neighbors in RGC mosaics. However, the electronics used in that experiment did not allow for patterned stimulation. By using the Stimchip it was possible, for the first time, to replicate the natural activity in a selected population of RGCs and to record the evoked activity at the level of single spikes.

At the same time, our results bring up some important issues for future investigations. First, the issue of an independent stimulation of RGCs of different types was not addressed in this study. Each RGC type is expected to form its own mosaic, but these mosaics will overlap and therefore the cell bodies of RGCs of different types may well be closely spaced, making an independent stimulation by a single electrode a significant challenge. This is an area of ongoing investigation, including the application of multielectrode stimulation to target individual RGCs (Jepson *et al* 2011).

Second, as noted in subsection 3.3, there can be a non-local, antidromic stimulation of a neuron. One consequence of this non-local stimulation is the crosstalk discussed in

subsection 3.4 and exhibited in figure 5, even in the case of stimulation of a mosaic of RGCs of a single type.

Third, although for the low-frequency stimulation used during the 'scan' procedure, we reliably and independently activated 12 out of 13 'OFF-1' cells (see section 3.3), replicating the natural activity of these RGCs required scaling up the stimulation currents by more than 50%. The net result was an unwanted initiation of action potentials in an axonal fiber of at least one 'OFF-1' RGC (see section 3.4). More generally, there is the issue of determining the optimal set of stimulation currents to replicate a desired pattern of spiking activity in a population of neurons with both high efficiency and minimal crosstalk. This is made even more challenging by the fact that the optimal stimulation currents may well depend on the recent past history of the applied stimulation pulses or the spiking activity of the neurons. We expect that the Stimchip, and the associated MEA system, will be an invaluable tool to investigate these and other issues related to the patterned stimulation of a neural population.

4.5. Future applications

For retinal prosthesis studies, we believe that it will be especially interesting to combine the Stimchip with arrays of high spatial density (Mathieson *et al* 2004, Gunning *et al* 2007). With the ability of such systems to stimulate RGCs with combinations of pulses generated by several closely spaced electrodes and with the simultaneous detection of the neurons' responses, it becomes possible to optimize techniques for the selective stimulation of the activity of small groups of neurons, or even individual cells. Furthermore, for an electrode array with high spatial density and high channel count, it would be possible to stimulate hundreds of many closely spaced RGCs in parallel, to record the evoked spiking activity, and thereby investigate methods to replicate arbitrarily defined patterns of activity in a large population of cells. Such stimulation schemes could be of high interest for the development of high-resolution retinal prostheses. For preliminary results on the application of the Stimchip to the studies on epiretinal prosthetic implants, see Jepson *et al* (2011).

For studies of neural networks, in brain tissue slices or intact brains, the stimulation of a population of neurons with complex spatiotemporal patterns of activity can be very useful in fundamental neuroscience research (Clarks *et al* 2011) as well as in biomedical applications, such as the development of multichannel neural prostheses (Fitzsimmons *et al* 2007) and deep brain stimulation techniques (Johnson *et al* 2008). It has recently been shown that the stimulation of activity of even a single neuronal cell *in vivo* can lead to detectable behavioral responses (Houweling and Brecht 2008) or change of the global brain state (Li *et al* 2009). It is also known that the activity of neural networks can show a high level of complexity (Beggs and Plenz 2003) and that the precise relative timing of action potentials in different neurons may encode important information in some neural systems (Gollisch and Meister 2008, Yang *et al* 2008). Consequently, one would like to stimulate the activity of a neural network with high spatial and temporal resolution and with a complexity and timing precision corresponding to the natural activity of the network. Unfortunately, the methods dedicated to the stimulation of individual neurons, using intracellular electrodes (Li *et al* 2009), or techniques based on juxtacellular labeling (Houweling and Brecht 2008) are hardly scalable to more than just a few neurons. On the other hand, it is still not well known how the brain circuits respond to the electrical stimulation with extracellular microelectrodes (for discussion see Histed *et al* 2009). Systems based on large-scale, high-density arrays of extracellular electrodes and the stimulator presented in this paper can help improve our understanding of the brain network's responses to complex microstimulation patterns and can be unique and very useful tools for studying information processing in such networks, in both *in vitro* and *in vivo* applications.

It is to be noted that a new technique for neural stimulation using optogenetics is under rapid development (Deisseroth 2011, Fenno *et al* 2011). This powerful method has the ability to target genetically tagged cell types and to silence as well as stimulate the neural activity with high spatial and temporal precision. It will be an important topic for future investigation and discussion to compare, and perhaps combine, optogenetics with electrical methods for the patterned stimulation, in both space and time, of neural systems.

5. Conclusions

The multichannel stimulation ASIC presented in this paper is a major step forward in the development of large-scale MEA systems for two-way communication with networks of neuronal cells. The Stimchip can provide independent stimulation signals to 64 electrodes in parallel and allows for the simultaneous recording of the network response with very low artifacts. In the pilot experiments, we were able, for the first time, to record short-latency spikes from stimulated neurons with minimal distortions even on the electrodes sending the stimulation currents and to replicate the natural spiking activity in a selected population of living neuronal cells. The chip is also compatible with various MEA designs and is suitable for building systems with several hundred independent channels (Hottowy *et al* 2010). The performance and flexibility of the Stimchip make it a very powerful tool for a broad variety of applications, including studies for the development of the next generation of retinal and neural prostheses and research in the field of fundamental neuroscience.

Acknowledgments

This work was supported by the Polish Ministry of Science and Higher Education and its grants for Scientific Research in the years 2009–2012 (WD), National Institutes of Health grant 5R21EB004410, National Science Foundation grant PHY-0750525 and the McKnight Foundation (AML) and Burroughs Wellcome Fund Career Award at the Scientific Interface (AS). DEG was funded through EPSRC LSI and RAEng fellowships. KM was funded through fellowships from the Royal Society of Edinburgh and the SU2P, an RCUK Science Bridges programme.

References

Anishchenko A, Greschner M, Elstrott J, Sher A, Litke A M, Feller M B and Chichilnisky E J 2010 Receptive field mosaics of retinal ganglion cells are established without visual experience *J. Neurophysiol.* **103** 1856–64

Beggs J M and Plenz D 2003 Neuronal avalanches in neocortical circuits *J. Neurosci.* **23** 11167–77 http://www.jneurosci.org/content/23/35/11167.full

Berdondini L, van der Wal P D, Guenat O, de Rooij N F, Koudelka-Hep M, Seitz P, Kaufmann R, Metzler P, Blanc N and Rohr S 2005 High-density electrode array for imaging *in vitro* electrophysiological activity *Biosens. Bioelectron.* **21** 167–74

Blanche T J, Spacek M A, Hetke J F and Swindale N V 2005 Polytrodes: high-density silicon electrode arrays for large-scale multiunit recording *J. Neurophysiol.* **93** 2987–3000

Brown E A, Ross J D, Blum R A, Nam Y, Wheeler B C and DeWeerth S P 2008 Stimulus-artifact elimination in a multi-electrode system *IEEE Trans. Biomed. Circuits Syst.* **2** 10–21

Buitenweg J R, Rutten W L C and Marani E 2002 Extracellular stimulation window explained by a geometry-based model of the neuron–electrode contact *IEEE Trans. Biomed. Eng.* **29** 1591–99

Charvet G *et al* 2010 BioMEA: a versatile high-density 3D microelectrode array system using integrated electronics *Biosens. Bioelectron.* **25** 1889–96

Clark K L, Armstrong K M and Moore T 2011 Probing neural circuitry and function with electrical microstimulation *Proc. R. Soc. Lond.* B **278** 1121–30

Csicsvari J, Henze D A, Jamieson B, Harris K D, Sirota A, Barthó P, Wise K D and Buzsáki G 2003 Massively parallel recording of unit and local field potentials with silicon-based electrodes *J. Neurophysiol.* **90** 1314–23

Dąbrowski W, Gryboś P, Hottowy P, Skoczeń A, Świentek K, Bezayiff N, Grillo A A, Kachiguine S, Litke A M and Sher A 2004 Development of integrated circuits for readout of microelectrode arrays to image neuronal activity in live retinal tissue *IEEE Nucl. Sci. Symp. Conf. Record (2003)* vol 2 pp 956–60

Dąbrowski W, Gryboś P, Hottowy P, Skoczeń A, Świentek K, Grillo A A, Kachiguine S, Litke A M and Sher A 2005 Development of front-end ASICs for imaging neuronal activity in live tissue *Nucl. Instrum. Methods Phys. Res.* A **541** 405–11

Deisseroth K 2011 Optogenetics *Nature Methods* **8** 26–9

Eversmann B *et al* 2003 A 128 × 128 CMOS biosensor array for extracellular recording of neural activity *IEEE J. Solid-State Circuits* **38** 2306–17

Fenno L, Yizhar O and Deisseroth K 2011 The development and application of optogenetics *Annu. Rev. Neurosci.* **34** 389–412

Field G D and Chichilnisky E J 2007 Information processing in the primate retina circuitry and coding *Annu. Rev. Neurosci.* **30** 1–30

Field G D *et al* 2010 *Nature* **467** 673–7

Fitzsimmons N A, Drake W, Hanson T L, Lebedev M A and Nicolelis M A L 2007 Primate reaching cued by multichannel spatiotemporal cortical microstimulation *J. Neurosci.* **27** 5593–602

Frey U *et al* 2010 Switch-matrix-based high-density microelectrode array in CMOS technology *IEEE J. Solid-State Circuits* **45** 467–82

Fried S I, Hsueh H A and Werblin F S 2006 A method for generating precise temporal patterns of retinal spiking using prosthetic stimulation *J. Neurophysiol.* **95** 970–8

Fried S I, Lasker A C W, Desai N J, Eddington D K and Rizzo J F 2009 Axonal sodium-channel bands shape the response to electric stimulation in retinal ganglion cells *J. Neurophysiol.* **101** 1972–7

Fujisawa S, Amarasingham A, Harrison M T and Buzsáki G 2008 Behavior-dependent short-term assembly dynamics in the medial prefrontal cortex *Nature Neurosci.* **11** 823–33

Gnadt J W, Echols S D, Yildirim A, Zhang H and Paul K 2003 Spectral cancellation of microstimulation artifact for simultaneous neural recording *in situ IEEE Trans. Biomed. Eng.* **50** 1129–35

Gollisch T and Meister M 2008 Rapid neural coding in the retina with relative spike latencies *Science* **319** 1108–11

Gryboś P, Dąbrowski W, Hottowy P, Fiutowski T and Bielewicz B 2006 Neuroplat64—low noise CMOS integrated circuit for neural recording applications *Proc. 5th Int. Meeting on Substrate-Integrated Micro Electrode Arrays (Reutlingen, Germany)* pp 208–9

Gunning D E, Chichilnisky E J, Litke A M, O'Shea V, Smith K M and Mathieson K 2007 Performance of ultra-high-density microelectrode arrays *Nucl. Instrum. Methods Phys. Res.* A **576** 215–9

Heer F, Hafizovic S, Ugniwenko T, Frey U, Franks W, Perriard E, Perriard J C, Blau A, Ziegler C and Hierlemann A 2007 Single-chip microelectronic system to interface with living cells *Biosens. Bioelectron.* **22** 2546–53

Histed M H, Bonin V and Reid R C 2009 Direct activation of sparse, distributed populations of cortical neurons by electrical microstimulation *Neuron* **63** 508–22

Hottowy P, Dąbrowski W, Kachiguine S, Skoczen A, Fiutowski T, Sher A, Rydygier P, Grillo A A and Litke A M 2008a An MEA-based system for multichannel, low artifact stimulation and recording of neural activity *Proc. 6th Int. Meeting on Substrate-Integrated Micro Electrode Arrays (Reutlingen, Germany)* pp 259–62

Hottowy P, Dąbrowski W, Skoczeń A and Wiącek P 2008b An integrated multichannel waveform generator for large-scale spatio-temporal stimulation of neural tissue *Analog Integr. Circuits Signal Process.* **55** 239–48

Hottowy P *et al* 2010 512-electrode MEA system for spatio-temporal distributed stimulation and recording of neural activity *Proc. 7th Int. Meeting on Substrate-Integrated Micro Electrode Arrays (Reutlingen, Germany)* pp 327–30

Houweling A R and Brecht M 2008 Behavioural report of single neuron stimulation in somatosensory cortex *Nature* **451** 65–8

Jensen R J, Rizzo J R, Ziv O R, Grumet A and Wyatt J 2003 Thresholds for activation of rabbit retinal ganglion cells with an ultrafine, extracellular microelectrode *Invest. Ophthalmol. Vis. Sci.* **44** 3533–43

Jepson L H, Hottowy P, Gunning D E, Mathieson K, Dąbrowski W, Litke A M and Chichilnisky E J 2011 Spatially patterned electrical stimulation of the retina for improved specificity *Proc. 5th Int. IEEE/EMBS Conf. Neural Engineering* pp 495–8

Jimbo Y, Kasai N, Torimitsu K, Tateno T and Robinson H P C 2003 A system for MEA-based multisite stimulation *IEEE Trans. Biomed. Eng.* **50** 241–8

Jochum T, Denison T and Wolf P 2009 Integrated circuit amplifiers for multi-electrode intracortical recording *J. Neural Eng.* **6** 012001

Johnson M D, Miocinovic S, McIntyre C C and Vitek J L 2008 Mechanisms and targets of deep brain stimulation in movement disorders *Neurotherapeutics* **5** 294–308

Li C T, Poo M M and Dan Y 2009 Burst spiking of a single cortical neuron modifies global brain state *Science* **324** 643–46

Litke A M 1999 The retinal readout system: a status report *Nucl. Instrum. Methods Phys. Res.* A **435** 242–9

Litke A M *et al* 2004 What does the eye tell the brain? Development of a system for the large scale recording of retinal output activity *IEEE Trans. Nucl. Sci.* **51** 1434–40

Mathieson K *et al* 2004 Large-area microelectrode arrays for recording of neural signals *IEEE Trans. Nucl. Sci.* **51** 2027–31

McAdams E T, Lackermeier A, McLaughlin J A and Macken D 1995 The linear and non-linear electrical properties of the electrode–electrolyte interface *Biosens. Bioelectron.* **10** 67–74

Merrill D R, Bikson M and Jefferys J G R 2005 Electrical stimulation of excitable tissue: design of efficacious and safe protocols *J. Neurosci. Methods* **141** 171–98

Petrusca D, Grivich M I, Sher A, Field G D, Gauthier J L, Greschner M, Shlens J, Chichilnisky E J and Litke A M 2007 Identification and characterization of a Y-like primate retinal ganglion cell type *J. Neurosci.* **27** 11019–27

Pillow J W, Shlens J, Paninski L, Sher A, Litke A M, Chichilnisky E J and Simoncelli E P 2008 Spatio-temporal correlations and visual signaling in a complete neuronal population *Nature* **454** 995–9

Rolston J D, Gross R E and Potter S M 2009 A low-cost multielectrode system for data acquisition enabling real-time closed-loop processing with rapid recovery from stimulation artifacts *Front. Neuroeng.* **2** doi:10.3389/neuro.16.012.2009

Sekirnjak C, Hottowy P, Sher A, Dąbrowski W, Litke A M and Chichilnisky E J 2006 Electrical stimulation of mammalian retinal ganglion cells with multielectrode arrays *J. Neurophysiol.* **95** 3311–27

Sekirnjak C, Hottowy P, Sher A, Dąbrowski W, Litke A M and Chichilnisky E J 2008 High-resolution electrical stimulation of primate retina for epiretinal implant design *J. Neurosci.* **28** 4446–56

Sekirnjak C, Hulse C, Jepson L H, Hottowy P, Sher A, Dąbrowski W, Litke A M and Chichilnisky E J 2009 Loss of responses to visual but not electrical stimulation in ganglion cells of rats with severe photoreceptor degeneration *J. Neurophysiol.* **102** 3260–9

Tang A *et al* 2008 A maximum entropy model applied to spatial and temporal correlations from cortical networks *in vitro* *J. Neurosci.* **28** 505–18

Tehovnik E J 1996 Electrical stimulation of neural tissue to evoke behavioral responses *J. Neurosci. Methods* **65** 1–17

Wagenaar D A, Pine J and Potter S M 2004 Effective parameters for stimulation of dissociated cultures using multi-electrode arrays *J. Neurosci. Methods* **138** 27–37

Wagenaar D A and Potter S M 2002 Real-time multi-channel stimulus artifact suppression by local curve fitting *J. Neurosci. Methods* **120** 113–20

Wagenaar D A and Potter S M 2004 A versatile all-channel stimulator for electrode arrays, with real-time control *J. Neural Eng.* **1** 39–45

Wichmann T 2000 A digital averaging method for removal of stimulus artifact in neurophysiologic experiments *J. Neurosci. Methods* **98** 57–62

Yang Y, DeWeese M R, Otazu G H and Zador A M 2008 Millisecond-scale differences in neural activity in auditory cortex can drive decisions *Nature Neurosci.* **11** 1262–3